Current **A**pplied **S**cience and **T**echnology e-ISSN: 2586-9396

Curr. Appl. Sci. Technol. 2026, Vol. 26 (No. 1), e0265899

Research article

Effects of Air, Vacuum, and Nitrogen Annealing on Structure, Bone Regeneration, and Antimicrobial Activity of Zinc-Doped Ca-P-O Microfibers

Siriwan Tocho[1], Arthit Ruttakorn[1], Chakkaphan Wattanawikkam[1,2] and Atipong Bootchanont[1,2]*

[1]Division of Physics, Faculty of Science and Technology, Rajamangala University of Technology Thanyaburi, Pathum Thani 12110, Thailand
[2]Smart Materials Research Unit, Division of Physics, Faculty of Science and Technology, Rajamangala University of Technology Thanyaburi, Pathum Thani 12110, Thailand

Received: 7 January 2025, Revised: 1 April 2025, Accepted: 1 April 2025, Published: 30 May 2025

Abstract

Calcium phosphate (CaP) is a family of materials closely resembling the mineral phase of natural bone and is widely used in bone tissue engineering for its biocompatibility and bioactivity. In this work, the starting material, Zn-doped calcium phosphate (Zn-CaP), was synthesized using the sol-gel method. Then, microfibers were fabricated using polyvinylpyrrolidone/Zn-CaP and the electrospinning technique. The samples were annealed under various conditions (air, vacuum, and nitrogen) at 800°C. The results indicated that the average fiber diameter ranged from 300 to 2000 microns, as observed by scanning electron microscopy (SEM). X-ray diffraction (XRD) analysis demonstrated that the main phase in air-annealed samples was calcium carbonate, with hydroxyapatite as the second phase. For vacuum annealing, the main phase was calcium carbonate, and the second phases were calcium oxide and hydroxyapatite, while nitrogen annealing resulted in an amorphous phase. Fourier transform infrared spectroscopy (FTIR) results were consistent with the XRD analysis. In addition, the local structure of Zn was investigated using X-ray absorption spectroscopy (XAS), which indicated the presence of a ZnO phase in air-annealed fibers and a ZnS phase in vacuum-annealed fibers. Nitrogen annealing resulted in an amorphous phase. Moreover, the simulated body fluid (SBF) immersion test results showed that the most significant formation of apatite layers occurred in nitrogen-annealed samples, enhancing the in vivo bone bioactivity of the microfibers. The antimicrobial activity results showed that the air and vacuum-annealed fibers demonstrated 100% effective against *Staphylococcus epidermidis* and *Pseudomonas aeruginosa*.

Keywords: bone regeneration; calcium phosphate; calcium carbonate; hydroxyapatite; microfiber; electrospinning; sol-gel process

*Corresponding author: E-mail: atipong_b@rmutt.ac.th
https://doi.org/10.55003/cast.2025.265899

1. Introduction

Osteoporosis is a condition caused by low bone density and reduced bone strength, which can lead to bones breaking easily. It is more common in patients aged 65 years and older and tends to lead to more health problems (Wolfson et al., 2009; Kumar & Maurya, 2018; Hawkins et al., 2021). The seriousness of osteoporosis and related conditions has fueled research in the field of bone tissue engineering, including the development of biomaterials and bioceramics, and the regeneration of defective bone tissue in human body (Hassan et al., 2022; Mankotia et al., 2023). However, it is important to create cell scaffolds for bone tissue engineering that mimic the hierarchical structure of the extracellular matrix and control the behavior of mesenchymal stem cells to optimize cell adhesion, proliferation, growth, and infiltration, including the diffusion of nutrients or waste products (Lao et al., 2011; Dong et al., 2018; Wijedasa et al., 2020).

Calcium phosphate (CaP), calcium carbonate ($CaCO_3$), and hydroxyapatite (HAp) are all widely studied materials for bone regeneration due to their biocompatibility and ability to support bone growth. Calcium phosphate, especially in the forms of hydroxyapatite and β-tricalcium phosphate (β-TCP), closely mimics the mineral components of natural bone. It exhibits excellent osteoconductivity and biodegradability, allowing it to integrate well with bone tissue. Researchers have focused on improving its mechanical properties and incorporating bioactive ions into it to enhance bone regeneration capabilities (Tavoni et al., 2021; Chen et al., 2023). $CaCO_3$ plays an important role in bone regeneration due to its biocompatibility, osteoconductive properties, and ability to provide a bioactive calcium source for new bone formation. It serves as a scaffold material that supports the growth and regeneration of bone tissue. $CaCO_3$ facilitates HAp deposition, promoting robust bone repair. Hydroxyapatite (HAp) is the primary mineral component of bone, known for forming a strong, bone-like material that integrates well with natural bone tissue (Wong et al., 2023; Min et al., 2024). HAp is a critical form of calcium phosphate, widely recognized for its close resemblance to the mineral component of human bone (Tripathi & Basu, 2012; Chen et al., 2023). It has uses in bone repair, bone grafting, cell scaffolding, and drug delivery. HAp has the necessary properties such as biocompatibility, bioactivity, biodigestibility, and bone induction to improve the biological response of surgical implants (Wei & Ma, 2004; Mondal et al., 2016). On the other hand, pure HAp exhibits less antibacterial activity. One challenge is to incorporate or dope metal ions like silver (Ag), zinc (Zn), titanium (Ti), and copper (Cu) into HAp to improve its anti-bacterial activity. These metal ions would provide better crystallinity as well as controlling bacterial adhesion. Zinc-doped calcium carbonate has emerged as a promising biomaterial in bone regeneration due to its synergistic effects in enhancing osteogenesis and antimicrobial properties. Zinc's antimicrobial properties help prevent infections at the implantation site, a critical factor in ensuring the success of bone grafts (O'Connor et al., 2020; Wen et al., 2023). Zinc ions exhibit excellent antibacterial properties, and numerous studies have shown that incorporating zinc ions can significantly enhance the antibacterial effectiveness of scaffolds (Chen et al., 2022). Özdemir and Yapar (2020) demonstrated that zinc can bind to the cell wall surface, interact with enzymes and proteins, and disrupt cell membranes by altering the secondary and tertiary structures of proteins.

To improve the scaffolds for bone tissue engineering, electrospinning is a prominent technique for creating nanofibrous scaffolds that support bone regeneration. These electrospun fibers closely mimic natural bone's extracellular matrix (ECM), providing a conducive environment for osteogenic cell growth and differentiation (Yan et al., 2022; Zhao et al., 2022). The fibers synthesized by electrospinning have attracted a lot of

attention as they are an effective means of producing a nonwoven membrane of nanofibers that has a high ratio of surface area to volume (Lee & Kim, 2014; Sebastian et al., 2020). The morphology of nanofibers can be tuned according to their fiber diameter with a fine and continuous micro-nanoscale by optimizing the polymer solution, synthesis process, and parameters (Dimassi et al., 2022; Kim et al., 2022). However, the synthesis of a Ca-P-O solution using the sol-gel method is the simplest method. It is based on the hydrolysis and condensation of the reactants to achieve the formation of colloidal particles (sols) and the formation of a three-dimensional network (gel) (Franco et al., 2012; Lee & Kim, 2014). However, various gas annealing processes for calcium phosphate microfiber have not been previously reported.

In this research, zinc-doped Ca-P-O microfibers were synthesized from calcium phosphate precursors using a sol-gel process with formation of fibers using polyvinylpyrrolidone (PVP) and an electrospinning process. The synthetic fibers, intended for use in bone replacement, were annealed under different environmental conditions (air, vacuum, and nitrogen). The fiber size, crystal structure, local structure, and the bio-stimulatory, and antibacterial activity of the fibers were investigated.

2. Materials and Methods

2.1 Materials

Triethylphosphate ($C_6H_{15}O_4P$), polyvinylpyrrolidone (PVP), and ethanol were purchased from Sigma-Aldrich Co., Ltd (USA). Calcium nitrate tetrahydrate ($CaN_2O_6{\cdot}4H_2O$) was obtained from Sigma-Aldrich Co., Ltd (India). Zinc nitrate hexahydrate ($Zn(NO_3)_2 \cdot 6H_2O$) was obtained from Sigma-Aldrich Co., Ltd (Germany). Other reagents and solvents were commercially available and were used as received.

2.2 Synthesis of calcium phosphate

Zn-doped hydroxyapatite was synthesized via the sol-gel method. The starting materials were weighed to achieve a Zn concentration of 3 mol% relative to Ca, using calcium nitrate tetrahydrate ($Ca(NO_3)_2{\cdot}4H_2O$, 99%, Sigma–Aldrich, Singapore) and zinc nitrate hexahydrate ($Zn(NO_3)_2{\cdot}6H_2O$, 98%, Sigma–Aldrich, Singapore). These precursors were dissolved in 100 mL of 2 M ethanol at ambient temperature and stirred continuously for 24 h. Triethyl phosphate (TEP, Sigma–Aldrich, Singapore) was added in a stoichiometric ratio to achieve a (Ca + Zn)/P molar ratio of 1.67. The TEP was hydrolyzed in a mixed ethanol–water solution (6:1 v/v) and stirred for 24 h at room temperature. The two solutions were then combined and stirred for 30 min, followed by aging at ambient temperature for 24 h. The resulting sol was subsequently heated at 50°C for 57 h to form a CaP solution, which was then used to synthesize calcium phosphate microfibers (Bootchanont et al., 2022).

2.3 Preparation of calcium carbonate microfibers

For the electrospinning of PVP/CaP composite membranes, 18 wt% of PVP was dissolved in ethanol. For the prepared electrospinning solutions, the concentration of PVP was adjusted to 90 w/v%, and the contents of CaP sol was 10 wt.%. All solutions for electrospinning were poured into a 10 mL syringe and fixed into an infusion pump. The solution was pushed manually with the syringe through the tube until the first drops could be seen on the needle tips, and then the flow rate was programmed, and the voltage and

the electrospinning process were initialized. The following electrospinning parameters were used: 10 cm tip-to-collector distance, 12 kV of power, and 1 mL/h of flow rate. All samples were calcined after the electrospinning process. An electrical furnace was used for the heat treatments. The heating profile used for fibers containing PVP was 1°C /min from 0°C to 350°C, and at 350°C, the temperature was held for 120 min to ensure complete dependability. Afterwards, the samples were heated up from 350°C to 800°C at a heating rate of 1°C /min for 10 h. All annealing processes were performed under air, vacuum, and nitrogen atmosphere (Sebastian et al., 2020).

2.4 Characterization of calcium carbonate microfibers

The fiber diameter and morphology after annealing were observed by a scanning electron microscope (SEM, JSM-5410LV, JEOL). Prior to SEM observation, all the samples were coated with gold using low-vacuum sputter coating. The average diameter of nanofibers was determined by analyzing the SEM images with image analyzing software (Image-Pro Plus, Media Cybernetics Inc., USA), and for the same samples of SEM, energy dispersive X-ray spectroscopy (EDX) was applied to detect the CaP sol distribution profile on the electrospun membrane surface and to analyze the changes in elemental composition of electrospun membranes due to the annealing (Lee & Kim, 2014).

XRD analysis was done on the samples using a Bruker D8 Advance Diffractometer and CuKα (λ = 0.15406 nm) radiation. The XRD measurements were conducted at a step rate of 0.02 nm/s within the range of 15-70^{o}.

FT-IR spectroscopy (Nicolet iS5, Thermo Fisher) was used to determine the chemical composition of the apatite mineralites on electrospun PVP fibrous scaffolds. For FT-IR measurement, a small amount of apatite powder from the microfibers synthesized was pressed into a transparent film (Kim et al., 2022).

X-ray absorption spectroscopy (XAS) technique performed on the Beamline 1.1 at the Synchrotron Light Research Institute (SLRI), Thailand, was used to explore the local information and oxidation state of zinc. The 19-channel Ge detector was used in the fluorescent mode of the XAS measurement. The available photon flux was in the range of 1–8 × 10^{9} photon/s, and the energy resolution is approximately 10^{-4}. The photon energy was chosen by spinning the double crystal monochromator (using Ge (220) crystals).

2.5 Simulated body fluid (SBF) immersion testing

The formation of bone-like apatite on the surface of prepared HAp microfibers was investigated in a simulated body fluid (SBF) with ion concentrations closely matching those of human blood plasma. The zinc-doped microfibers, annealed in air, vacuum, and nitrogen, were placed in a container for immersion in the body simulation solution. The solution was poured into the container until it fully covered the zinc-doped calcium carbonate microfibers, then maintained at 37°C for two weeks (Lee & Kim, 2014).

2.6 Antibacterial activity

The antibacterial activity of the experimental samples was tested against gram-positive bacteria *Staphylococcus epidermidis* and gram-negative bacteria *Pseudomonas aeruginosa* obtained from Thailand Institute of Scientific and Technological Research (TISTR).

A 0.05 g portion of each tested substance was placed into a test tube containing 2.5 mL of 1% peptone and sterilized by autoclaving at 121°C for 15 min. Bacterial starters of *S. epidermidis* and *P. aeruginosa* were prepared in tryptic soy broth (TSB) at 37°C for 24 h prior to testing. Subsequently, each bacterial culture was diluted with sterile buffer to achieve an initial concentration of approximately Log 7 CFU/mL. Fifty microliters of each prepared starter culture were pipetted into the test tubes containing the treated substances.

In addition, 50 µL of each starter culture was pipetted into sterile test tubes without the tested substances to serve as positive controls. Each treatment was performed in triplicate. All samples were incubated at 37°C for 1 h, following the ASTM E2149-20 standard method. Serial dilutions of each sample were performed using 0.85% NaCl solution and spread on tryptic soy agar (TSA). Plates were incubated at 37°C for 24 h. The percent reduction of pathogenic bacteria by the tested substances was calculated based on the average colony-forming units per milliliter (CFU/mL) of the positive control (B) and the treated sample (A) using the following formula (Supanwong & Nounurai, 2020).

$$\text{Reduction, } \%\,(\text{CFU/mL}) = \frac{B-A}{B} \times 100 \quad (1)$$

3. Results and Discussion

3.1 Crystal structure analysis with an X-ray diffractometer (XRD)

X-ray diffraction patterns of zinc-doped Ca-P-O microfibers that had been annealed in air, vacuum, and nitrogen at 350°C for 2 h and then further annealed with increase of temperature to 800°C for 10 h, are shown in Figure 1. For the zinc-doped Ca-P-O microfibers annealed in the air (3%Zn-air), the main phase identified was calcium carbonate, with hydroxyapatite as the secondary phase (JCPDS file no. 10-072-01937, 00-024-0030, 96-900-2215). In the case of vacuum-annealed microfibers (3% Zn-vacuum), calcium carbonate remained the primary phase, while calcium oxide and hydroxyapatite were identified as secondary phases (JCPDS file no. 01-086-2339, 96-900-6714). Meanwhile, the zinc-doped Ca-P-O microfibers annealed in nitrogen (3% Zn-nitrogen) resulted in an amorphous phase. This result shows the effect of air on forming the calcium phosphate group.

Additionally, the Scherrer equation was used to calculate the crystallite sizes of the samples, and the results are presented in Table 1. For the samples annealed in air, the main diffraction peaks of $CaCO_3$ and HAp indicate crystallite sizes of 33.49 nm and 34.53 nm, respectively. In contrast, the samples annealed in vacuum exhibit crystallite sizes of 36.99 nm and 33.66 nm for $CaCO_3$ and HAp, respectively. These results indicate that annealing conditions (air vs. vacuum) do not significantly affect the crystallite size (Sronsri et al., 2020).

3.2 Analysis of the chemical structural components of substances using FTIR

The chemical structure analysis for phosphate (PO_4^{3-}), calcium carbonate ($CaCO_3$), and hydroxyl (OH^-) groups in the fibers annealed at 800°C under air, vacuum, and nitrogen atmospheres was performed using Fourier Transform Infrared (FTIR) spectroscopy, and the results are presented in Figure 2.

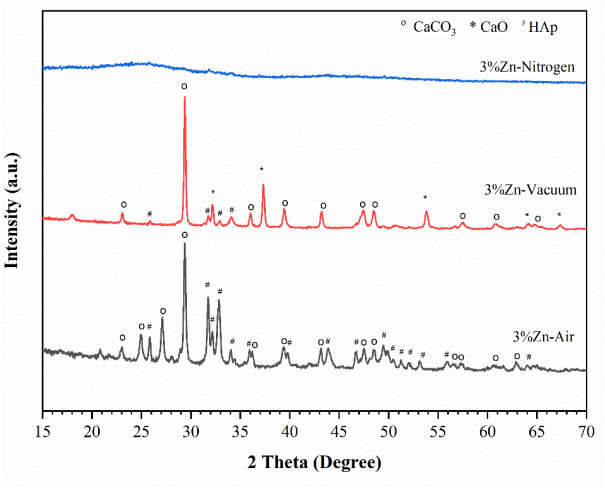

Figure 1. X-ray diffraction patterns of 3%Zn-air, 3%Zn-vacuum, and 3%Zn-nitrogen

Table 1. The crystal size calculated from the Scherrer equation

Samples	Phase	2Θ (degree)	FWHM (radian)	Crystallite Size (nm)
3%Zn-Air	$CaCO_3$	29.38	0.26	33.49
	HAp	31.75	0.23	34.53
3%Zn-Vacuum	$CaCO_3$	29.39	0.22	36.99
	HAp	31.77	0.24	33.66

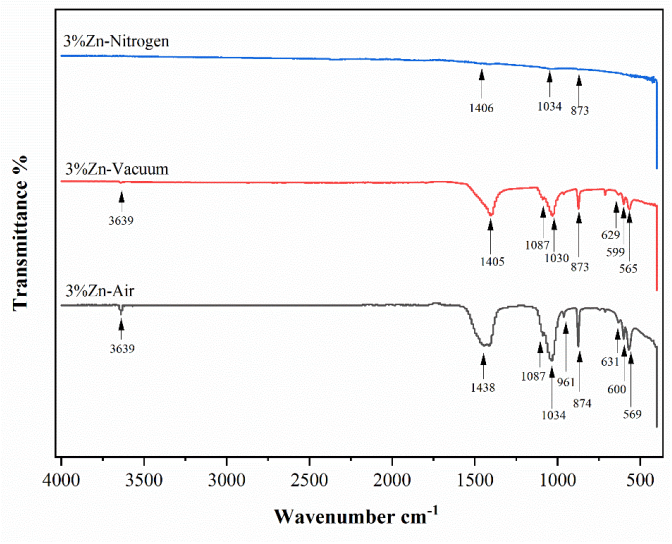

Figure 2. Fourier transform infrared spectra of 3%Zn-Air, 3%Zn-Vacuum, and 3%Zn-Nitrogen

For the 3% Zn-Air sample, the wide bands at approximately 1000 and 1100 cm^{-1} indicate the formation of an apatite structure. The bands resulted from the symmetric deformation of hydroxyl groups are at 3639 and 631 cm^{-1}, while the absorption bands corresponding to $CaCO_3$ vibrations appear at about 1438 and 874 cm^{-1}. Additionally, the absorption bands for PO_4^{3-} are observed at around 1087, 1034, 961, 600, and 569 cm^{-1}. In the 3% Zn-vacuum sample, the bands assigned to hydroxyl groups are detected at 3639 and 629 cm^{-1}. The vibrational bands of $CaCO_3$ appeared at approximately 1405 and 873 cm^{-1}, and the PO_4^{3-} absorption bands are identified at around 1087, 1030, 599, and 565 cm^{-1}. For the 3% Zn-nitrogen sample, the absorption bands for $CaCO_3$ vibrations are observed at about 1406 and 873 cm^{-1}, while the PO_4^{3-} absorption band appears at around 1034 cm^{-1}. The FTIR analysis confirmed the formation of Ca-P-O microfibers, and the results were in compatible with the XRD analysis results.

3.3 Investigation of the local structure using X-ray absorption spectroscopy (XAS)

X-ray Absorption Near-Edge Structure (XANES) primarily measures the excitation of core electrons to unoccupied states, providing insights into the local electronic structure. This process generates spherical electron waves that get scattered by neighboring atoms, enabling the analysis of the local chemical environment around the absorbing atom. This technique allows researchers to determine details such as oxidation states, coordination geometry, and bond arrangements (Bootchanont et al., 2020).

The normalized Zn K-edge XANES spectra for 3% Zn-air, 3% Zn-vacuum, and 3% Zn-nitrogen samples compared with the standard of Zn foil, ZnO, and ZnS spectra are presented in Figure 3, where the absorption edge is observed at approximately 9661 eV, indicating the presence of Zn^{2+} ions in all samples. The spectral features provide insight into the local coordination and oxidation state of zinc in the different samples. For the 3% Zn-air sample, the XANES spectrum clearly reveals characteristics corresponding to the ZnO phase, suggesting the formation of crystalline ZnO under air conditions. In contrast, the 3% Zn-vacuum sample exhibits spectral features indicative of the ZnS phase, highlighting the impact of the vacuum environment on the structural evolution of the material. However, the 3% Zn-nitrogen sample presents ambiguous spectral features that cannot be conclusively attributed to a crystalline structure. This result, combined with the XRD findings, suggests the presence of an amorphous phase in the nitrogen-treated sample. The absence of distinct spectral features typically associated with crystalline ZnO or ZnS further supports this interpretation.

3.4 The microstructural analysis with the scanning electron microscope (SEM)

Microstructural characterization of the zinc-doped Ca-P-O microfibers annealed in air, vacuum, and nitrogen was conducted. The fibers were annealed at 350°C for 2 h, followed by an increase in temperature to 800°C for 10 h. The samples were examined using a scanning electron microscope (SEM) at 5000x magnification, and then the diameter of the fibers was measured using the ImageJ program at 30 different positions in the SEM image, as shown in Figure 4. The 3% Zn-air sample showed an average fiber size of 0.898-2.157 μm. The fibers appear rough, with relatively large diameters, resulting in less porosity between the fibers. Continuous fibers were formed by the decomposition and evaporation

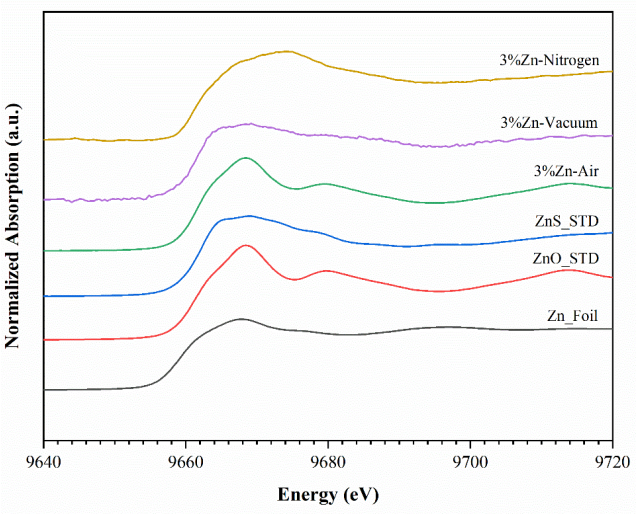

Figure 3. Normalized Zn K-edge XANES spectra of Zn foil, ZnO standard, ZnS standard, 3%Zn-air, 3%Zn-vacuum, and 3%Zn-nitrogen

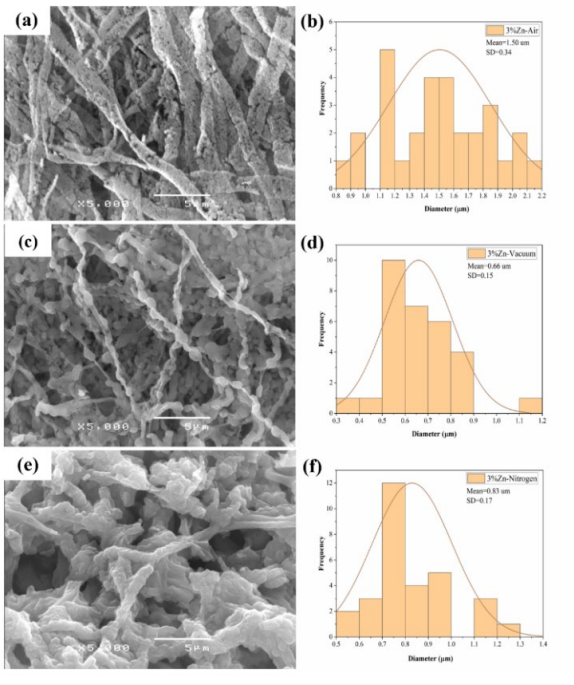

Figure 4. Scanning electron micrographs and microfiber diameter distribution of zinc-doped Ca-P-O microfibers annealed in different environments, namely air, vacuum, and nitrogen as follows: (a), (b) 3%Zn-air, (c), (d) 3%Zn-vacuum, and (e), (f) 3%Zn-nitrogen

of the PVP solution (Figure 4a, b). In contrast, the 3% Zn-vacuum sample exhibits a more porous structure between the fibers. The fibers appear as beads or bead-like structures, typically generated by electrospinning with low-viscosity solutions (Ren et al., 2010). The average fiber size is 0.342-0.626 μm (Figure 4c, d). For the 3% Zn-nitrogen sample, the fibers formed lumps and presented the least porous structure, with an average fiber size of 0.559-0.785 μm (Figure 4e, f).

3.5 Simulated body fluid (SBF) immersion

The key requirement for an artificial material to bond with living bone is the formation of a bone-like apatite layer on its surface when implanted in the body. This process of apatite formation in vivo can also be replicated in a simulated body fluid (SBF) with ion concentrations nearly identical to those of human blood plasma (Lee & Kim, 2014).

Scanning electron microscopy (SEM) images of the cell culture scaffold surfaces treated with SBF for 14 days are shown in Figure 5. The 3% Zn-air sample showed clear apatite layer formation, but some pores and fibers remained uncovered by the apatite layer (Figure 5a). The 3% Zn-vacuum sample displayed apatite deposition at certain points on the fiber surface. Spherical-like particles agglomerated into clusters, leaving many pores visible and the fibers largely uncovered by the apatite layer (Figure 5b). In contrast, the 3% Zn-nitrogen sample exhibited a fully covered surface with an apatite layer consisting of nanosheets self-assembled into three-dimensional structures. The underlying nanofibers were no longer observable, and the membrane's pores were clogged due to significant crystal growth (Figure 5c). Therefore, the 3% Zn-nitrogen sample showed an apatite layer well even on an amorphous structure (Braga et al., 2014).

3.6 Energy dispersive X-ray spectroscopy (EDS)

The results of energy-dispersive X-ray spectroscopy (EDX) confirm the presence of zinc in samples immersed in simulated body fluid (SBF) for 14 days. Table 2 shows the zinc content in the samples, with the highest zinc content found in those annealed under air, vacuum, and nitrogen.

Calcium and phosphate are the main components that form the apatite layer. While hydroxyapatite (HAp) has a Ca:P ratio of 1.67, bone minerals have Ca:P ratios ranging from 1.37 to 1.87. This variation is due to the more complex composition of bone minerals, which include additional ions such as silicon, carbonate, and zinc (Hughes et al., 2019; Wan et al., 2022).

Table 2 presents the elemental composition determined by EDX analysis, showing the presence of elements and the Ca: P ratio in samples immersed in SBF for 14 days. The 3% Zn-air sample contained a zinc content of 0.71 and a Ca:P ratio of 5.18, indicating reduced apatite formation, with calcium dominating the structure (Figure 5a). The 3% Zn-vacuum sample had a zinc content of 0.05 and a Ca:P ratio of 50.03, suggesting excessive calcium formation and limited apatite layer development (Figure 5b). In contrast, the 3% Zn-nitrogen sample contained a zinc content of 0.03 and a Ca:P ratio of 1.92, which closely aligns with the Ca:P ratio of natural bone. This sample also exhibited the best formation and distribution of the apatite layer on the fibers (Figure 5c).

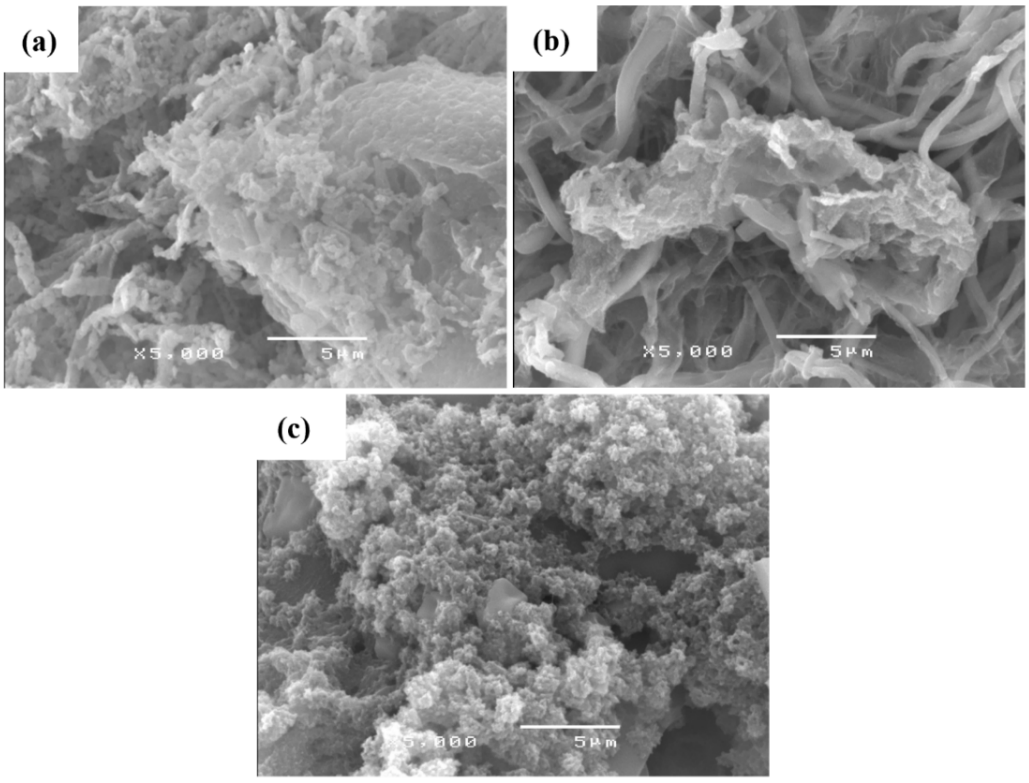

Figure 5. Scanning electron microscopy (SEM) images of the cell culture scaffold surface treated with simulated body condition (SBF) for 14 days as follows: (a) 3%Zn-air, (b) 3%Zn-vacuum, and (c) 3%Zn-nitrogen

Table 2. X-ray energy distribution of zinc-doped Ca-P-O microfibers after immersion in simulated body fluid (SBF) for 14 days as follows: 3%Zn-air, 3%Zn-vacuum, and 3%Zn-nitrogen

Elements	3%Zn-Air (Atomic%)	3%Zn-Vacuum (Atomic %)	3%Zn-Nitrogen (Atomic %)
Ca	22.67	55.03	8.47
O	51.82	29.90	37.93
P	4.38	1.10	4.42
Zn	0.71	0.05	0.03
Cl	1.74	2.14	9.33
Ca/P	5.18	50.03	1.92

3.7 Evaluation of antibacterial activity

The antimicrobial tests of zinc-doped Ca-P-O microfibers annealed in air, vacuum, and nitrogen against *S. epidermidis* and *P. aeruginosa* are shown in Figure 6. The results indicate that the 3% Zn-air and 3% Zn-vacuum samples were 100% effective against both *S. epidermidis* and *P. aeruginosa*. In contrast, the 3% Zn-nitrogen sample was 64.29% effective against *S. epidermidis* and 65.63% effective against *P. aeruginosa.* This reduced effectiveness may be attributed to the zinc amorphous phase in the 3% Zn-nitrogen sample. These experimental results confirm that ZnO and ZnS significantly enhance antibacterial activity. However, the cytotoxic effects of ZnO and ZnS on cells may limit their suitability for applications in bone tissue engineering (Alfata et al., 2020; Bouasla et al., 2024).

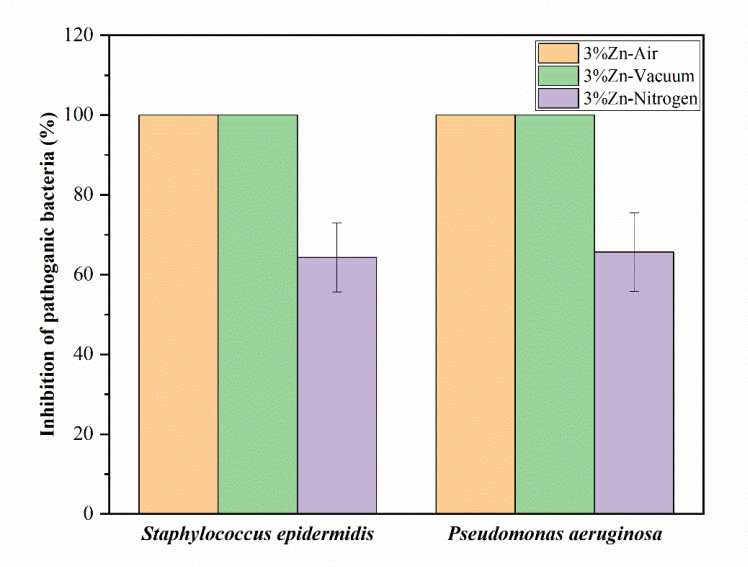

Figure 6. Antimicrobial tests of zinc-doped Ca-P-O microfibers calcined in different environments: air, vacuum, and nitrogen, against bacteria *S. epidermidis* and *P. aeruginosa*

4. Conclusions

The Ca-P-O microfibers annealed in air, vacuum, and nitrogen from zinc-doped calcium phosphate (Zn-CaP) were synthesized using the sol-gel method. The fibers were formed using electrospinning of polyvinylpyrrolidone (PVP). The synthesized samples were calcined at 800°C under different environmental conditions to investigate their crystal structure, fiber size, and their biostimulatory, and antimicrobial properties. X-ray diffraction (XRD) analysis revealed that the fibers annealed in air (3% Zn-air) primarily consisted of calcium carbonate, with hydroxyapatite as a secondary phase. For the fibers annealed in vacuum (3% Zn-vacuum), calcium carbonate was the main phase, followed by calcium oxide and hydroxyapatite. In contrast, the fibers annealed in nitrogen (3% Zn-Nitrogen) formed an amorphous phase. X-ray absorption spectroscopy (XAS) indicated the presence of the ZnO phase in the air-annealed fibers and the ZnS phase in the vacuum-annealed fibers. The nitrogen-annealed fibers showed an amorphous phase. Scanning electron

microscopy (SEM) revealed that the fibers were micrometer-sized. Energy dispersive X-ray spectroscopy (EDX) confirmed the presence of zinc and provided the calcium-to-phosphate (Ca:P) ratio. After immersion in simulated body fluid (SBF) for 14 days, the nitrogen-annealed (3% Zn-nitrogen) fibers demonstrated the best apatite layer formation. The fibers annealed under air (3% Zn-Air) and vacuum (3% Zn-Vacuum) conditions showed 100% antimicrobial activity against *S. epidermidis* and *P. aeruginosa.*

5. Acknowledgements

This research work received funding support from the NRFS via the Program Management Unit for Human Resources and Institutional Development Research and Innovation (grant number B05F640090). The authors would like to thank the computing resources provided by the Computational Materials Physics Project, SLRI, Thailand, Rajamangala University of Technology ISAN, and Rajamangala University of Technology Thanyaburi.

6. Author Contributions

Siriwan Tocho: Writing – original draft, methodology, ınvestigation. Arthit Ruttakorn: Methodology, ınvestigation. Chakkaphan Wattanawikkam: Writing – review & editing, ınvestigation, formal analysis. Atipong Bootchanont: Writing – review & editing, ınvestigation, formal analysis, conceptualization.

7. Conflicts of Interest

There are no conflicts to declare.

ORCID

Atipong Bootchanont https://orcid.org/0000-0002-3718-761X

Chakkaphan Wattanawikkam https://orcid.org/0000-0002-5902-5312

References

Alfata, R., Ramahdita, G., & Yuwono, A. H. (2020). The effect of additional zinc oxide to antibacterial property of chitosan/collagen-based scaffold. *Materials Science Forum*, 1000, 107-114.

Bootchanont, A., Wechprasit, T., Areesamarn, N., Pholprom, R., Hwangphon, T., Temprom, L., Amonpattaratkit, P., Klysubun, W., & Yimnirun, R. (2020). Comparison of local structure between Mg/Mn-doped natural and synthetic hydroxyapatites by X-ray absorption spectroscopy. *Radiation Physics and Chemistry*, 177, Article 109075. https://doi.org/10.1016/j.radphyschem.2020.109075

Bootchanont, A., Wechprasit, T., Isran, N., Theangsunthorn, J., Chaosuan, N., Chanlek, N., Kidkhunthod, P., Yimnirun, R., Jiamprasertboon, A., Eknapakul, T., Siritanon, T., Sailuam, W., & Saisopa, T. (2022). Correlation of the antibacterial activity and local structure in Zn- and Mn-doped hydroxyapatites by Rietveld refinement and the first-principles method. *Materialia*, 26, Article 101586. https://doi.org/10.1016/j.mtla.2022.101586

Bouasla, N., Abderrahmane, S., Obeizi, Z., Sarah, M., & Saoudi, A. (2024). Antimicrobial Activity of ZnS and ZnO-TOP nanoparticles againts pathogenic bacteria. *Chemistry and Biodiversity*, 21(12), Article e202400724. https://doi.org/10.1002/cbdv.202400724

Braga, F., da Silva, A. C., Allegrini, S. Jr, & Ottoni, C. (2014). Calcium phosphate graft substitute: When the impact of innovation is in the form rather than content. In *Proceedings of 26th European conference on biomaterials* (pp. 1-12). European Society for Biomaterials.

Chen, X., Li, H., Ma, Y., & Jiang, Y. (2023). Calcium phosphate-based nanomaterials: preparation, multifunction, and application for bone tissue engineering. *Molecules*, 28(12), Article 4790. https://doi.org/10.3390/molecules28124790

Chen, Z., Zhang, W., Wang, M., Backman, L. J., & Chen, J. (2022). Effects of zinc, magnesium, and iron ions on bone tissue engineering. *ACS Biomaterials Science and Engineering*, 8(6), 2321-2335. https://doi.org/10.1021/acsbiomaterials.2c00368

Dimassi, S., Tabary, N., Chai, F., Zobrist, C., Hornez, J.-C., Cazaux, F., Blanchemain, N., & Martel, B. (2022). Polydopamine treatment of chitosan nanofibers for the conception of osteoinductive scaffolds for bone reconstruction. *Carbohydrate Polymers*, 276, Article 118774. https://doi.org/10.1016/j.carbpol.2021.118774

Dong, Y., Liang, J., Cui, Y., Xu, S., & Zhao, N. (2018). Fabrication of novel bioactive hydroxyapatite-chitosan-silica hybrid scaffolds: Combined the sol-gel method with 3D plotting technique. *Carbohydrate polymers*, 197, 183-193. https://doi.org/10.1016/j.carbpol.2018.05.086

Franco, P. Q., João, C. F. C., Silva, J. C., & Borges, J. P. (2012). Electrospun hydroxyapatite fibers from a simple sol–gel system. *Materials Letters*, 67(1), 233-236. https://doi.org/10.1016/j.matlet.2011.09.090

Hassan, M., Sulaiman, M., Yuvaraju, P. D., Galiwango, E., Rehman, I. U., Al-Marzouqi, A. H., Khaleel, A., & Mohsin, S. (2022). Biomimetic PLGA/strontium-zinc nano hydroxyapatite composite scaffolds for bone regeneration. *Journal of Functional Biomaterials*, 13(1), Article 13. https://doi.org/10.3390/jfb13010013

Hawkins, F., Garla, V., Allo, G., Males, D., Mola, L., & Corpas, E. (2021). Senile and postmenopausal osteoporosis: Pathophysiology, diagnosis, and treatment. In E. Corpas (Ed.). *Endocrinology of aging* (pp. 131-169). Elsevier. https://doi.org/10.1016/B978-0-12-819667-0.00005-6

Hughes, E. A., Robinson, T. E., Bassett, D. B., Cox, S. C., & Grover, L. M. (2019). Critical and diverse roles of phosphates in human bone formation. *Journal of Materials Chemistry B*, 7(47), 7460-7470. https://doi.org/10.1039/C9TB02011J

Kim, J. I., Kim, J. Y., Kook, S.-H., & Lee, J.-C. (2022). A novel electrospinning method for self-assembled tree-like fibrous scaffolds: Microenvironment-associated regulation of MSC behavior and bone regeneration. *Journal of Materials Science and Technology*, 115, 52-70. https://doi.org/10.1016/j.jmst.2021.10.039

Kumar, S., & Maurya, R. (2018). Plant drugs in the treatment of osteoporosis. In S. C. Mandai, V. Mandal, & T. Konishi (Eds.). *Natural Products and Drug Discovery* (pp. 179-212). Elsevier. https://doi.org/10.1016/B978-0-08-102081-4.00008-3

Lao, L., Wang, Y., Zhu, Y., Zhang, Y., & Gao, C. (2011). Poly (lactide-co-glycolide)/hydroxyapatite nanofibrous scaffolds fabricated by electrospinning for bone tissue engineering. *Journal of Materials Science: Materials in Medicine*, 22, 1873-1884. https://doi.org/10.1007/s10856-011-4374-8

Lee, J.-H., & Kim, Y.-J. (2014). Hydroxyapatite nanofibers fabricated through electrospinning and sol–gel process. *Ceramics International*, 40(2), 3361-3369. https://doi.org/10.1016/j.ceramint.2013.09.096

Mankotia, P., Sharma, K., Sharma, V., Sehgal, R., & Kumar, V. (2023). Inorganic bionanocomposites for bone tissue engineering. In M. S. Hasnain, A. K. Nayak, & T. M. Aminabhavi (Eds.). *Inorganic Nanosystems* (pp. 589-619). Elsevier. https://doi.org/10.1016/B978-0-323-85784-0.00013-3

Min, K. H., Kim, D. H., Kim, K. H., Seo, J.-H., & Pack, S. P. (2024). Biomimetic scaffolds of calcium-based materials for bone regeneration. *Biomimetics*, 9(9), Article 511. https://doi.org/10.3390/biomimetics9090511

Mondal, S., Pal, U., & Dey, A. (2016). Natural origin hydroxyapatite scaffold as potential bone tissue engineering substitute. *Ceramics International*, 42(16), 18338-18346. https://doi.org/10.1016/j.ceramint.2016.08.165

O'Connor, J. P., Kanjilal, D., Teitelbaum, M., Lin, S. S., & Cottrell, J. A. (2020). Zinc as a therapeutic agent in bone regeneration. *Materials*, 13(10), Article 2211. https://doi.org/10.3390/ma13102211

Özdemir, G., & Yapar, S. (2020). Preparation and characterization of copper and zinc adsorbed cetylpyridinium and N-lauroylsarcosinate intercalated montmorillonites and their antibacterial activity. *Colloids and Surfaces B: Biointerfaces*, 188, Article 110791. https://doi.org/10.1016/j.colsurfb.2020.110791

Ren, L., Wang, J., Yang, F.-Y., Wang, L., Wang, D., Wang, T.-X., & Tian, M.-M. (2010). Fabrication of gelatin–siloxane fibrous mats *via* sol–gel and electrospinning procedure and its application for bone tissue engineering. *Materials Science and Engineering: C*, 30(3), 437-444. https://doi.org/10.1016/j.msec.2009.12.013

Sebastian, T., Preisker, T., Gorjan, L., Graule, T., Aneziris, C., & Clemens, F. (2020). Synthesis of hydroxyapatite fibers using electrospinning: A study of phase evolution based on polymer matrix. *Journal of the European Ceramic Society*, 40(6), 2489-2496. https://doi.org/10.1016/j.jeurceramsoc.2020.01.070

Sronsri, C., Kongpop, U., & Sittipol, W. (2020). Quantitative analysis of calcium carbonate formation in magnetized water. *Materials Chemistry and Physics*, 245(3), Article 122735. https://doi.org/10.1016/j.matchemphys.2020.122735

Supanwong, K., & Nounurai, P. (2020). Identification and elimination of errors in the drop plate counts. *Maejo International Journal of Science and Technology*, 14(3), 252-260.

Tavoni, M., Dapporto, M., Tampieri, A., & Sprio, S. (2021). Bioactive calcium phosphate-based composites for bone regeneration. *Journal of Composites Science*, 5(9), Article 227. https://doi.org/10.3390/jcs5090227

Tripathi, G., & Basu, B. (2012). A porous hydroxyapatite scaffold for bone tissue engineering: Physico-mechanical and biological evaluations. *Ceramics International*, 38(1), 341-349. https://doi.org/10.1016/j.ceramint.2011.07.012

Wan, B., Ruan, Y., Shen, C., Xu, G., Forouzanfar, T., Lin, H., & Wu, G. (2022). Biomimetically precipitated nanocrystalline hydroxyapatite. *Nano TransMed*, 1(2-4), Article e9130008. https://doi.org/10.26599/NTM.2022.9130008

Wei, G., & Ma, P. X. (2004). Structure and properties of nano-hydroxyapatite/polymer composite scaffolds for bone tissue engineering. *Biomaterials*, 25(19), 4749-4757. https://doi.org/10.1016/j.biomaterials.2003.12.005

Wen, X., Wang, J., Pei, X., & Zhang, X. (2023). Zinc-based biomaterials for bone repair and regeneration: mechanism and applications. *Journal of Materials Chemistry B*, 11, 11405-11425. https://doi.org/10.1039/D3TB01874A

Wijedasa, N. P., Broas, S. M., Daso, R. E., & Banerjee, I. A. (2020). Varying fish scale derived hydroxyapatite bound hybrid peptide nanofiber scaffolds for potential applications in periodontal tissue regeneration. *Materials Science and Engineering: C*, 109, Article 110540. https://doi.org/10.1016/j.msec.2019.110540

Wolfson, E. M., DeKalb, A., & Rojhani, A. (2009). Women's health in the 21st century.*International Journal of Gynecology and Obstetrics*, 104, S2-S3. https://doi.org/10.1016/j.ijgo.2008.11.029

Wong, S. K., Yee, M. M. F., Chin, K.-Y., & Ima-Nirwana, S. (2023). A review of the application of natural and synthetic scaffolds in bone regeneration. *Journal of Functional Biomaterials*, 14(5), Article 286. https://doi.org/10.3390/jfb14050286

Yan, X., Yao, H., Luo, J., Li, Z., & Wei, J. (2022). Functionalization of electrospun nanofiber for bone tissue engineering. *Polymers*, 14(14), Article 2940. https://doi.org/10.3390/polym14142940

Zhao, T., Zhang, J., Gao, X., Yuan, D., Gu, Z., & Xu, Y. (2022). Electrospun nanofibers for bone regeneration: from biomimetic composition, structure to function. *Journal of Materials Chemistry B*, 10(32), 6078-6106. https://doi.org/10.1039/D2TB01182D